IEEE Access
Multidisciplinary | Rapid Review | Open Access Journal

Received May 14, 2018, accepted June 14, 2018, date of publication June 18, 2018, date of current version July 6, 2018.

Digital Object Identifier 10.1109/ACCESS.2018.2848841

Stacked Auto-Encoder Based Fault Location in VSC-HVDC

GUOMIN LUO[1], CHANGYUAN YAO[1], YINGLIN LIU[1], YINGJIE TAN[1], JINGHAN HE[1], AND KAI WANG[2]

[1]School of Electrical Engineering, Beijing Jiaotong University, Beijing 100044, China
[2]CloudMinds Technologies Inc., Beijing 100102, China

Corresponding author: Guomin Luo (guominluo@hotmail.com)

This work was supported in part by the National Natural Science Foundation of China under Grant 51507008, in part by the National Key Research and Development Program of China under Grant 2017YFB0902800, and in part by the Fundamental Research Funds for the Central Universities under Grant 2018JBM056.

ABSTRACT This paper presents an end-to-end approach for locating faults on high-voltage dc (HVDC) transmission lines. Different from traditional methods which rely on communications between different measuring units or feature extraction of post fault transients, the proposed algorithm takes the raw data of locally detected traveling current surges as the only-input and outputs the fault locations directly. Especially, the stacked auto-encoder (SAE) is utilized to model the relationship between fault currents and fault locations. The SAE-based method is performed in time domain and tested with a simulated HVDC transmission line modeled in PSCAD/EMTDC. The simulation results show that this method is effective in locating faulted points and robust against attenuation, overlapping of traveling surges, and various ground resistances.

INDEX TERMS VSC-HVDC, fault location, stacked auto-encoder, deep learning.

I. INTRODUCTION

Considering a number of advantages, such as lower loss, larger transmission capacity and lower insulation requirement, high-voltage DC (HVDC) is a preferred choice for long distance power transmission [1]. The wide use of an insulated gate bipolar transistor (IGBT) and pulse-width modulation (PWM) accelerates the development of voltage-source convertors (VSCs), which provide high reliability and flexible control of power flow. Such a development attracts more researchers to focus on VSC-based HVDC [2].

Accurate fault location can help engineers to find the faulted area and recover the system in a short time [3]. The two main approaches are usually used in HVDC systems to find the faulted locations: the fault feature-based methods and the traveling wave-based methods. Each has some advantages and shortcomings.

The fault feature-based methods usually study the fault loops or the variations of post-fault measurements [4]. The post-fault response of VSC DC system includes three phases: (a) capacitor discharging phase; (b) diode freewheel phase; (c) grid current-fed phase. In phase (a), the supporting capacitor discharges and the electrical measurements depend mainly on the topology and structure of transmission lines. In phase (b), the currents in IGBT increases and trips the controllers to block IGBTs out. In phase (c), currents flow from AC sources to DC faults via diodes. Both phase (a) and phase (c) can be modeled with linear systems and are often used in fault location analysis. With transmission line parameters, the fault feature based methods can calculate the fault locations with the post-fault measurements in fault loops. Time domain operations such as root mean square (RMS) values of both AC and DC measurements [5]–[8], frequency domain extractions such as harmonic frequency components [4], [9], [10], and time-frequency distributions such as Hilbert-Huang transform (HHT) or wavelet transform represented features [2], [11], [12] have all been considered. These methods show good performance in a lot of experimental scenarios, while challenges still exist in practical applications due to the lack of accurate line parameters.

The traveling wave (TW) analysis methods are most commonly used in practical projects. Once the first TW reaches line terminal, the post-fault response of DC convertors will start. So, the TW based methods, especially the ones with wave fronts, will not be affected by convertor controllers. The wave fronts are usually captured at one or more terminals. The single-end traveling wave methods usually capture

the arriving time of incident wave and reflected wave and realize the fault location with the time difference [13]–[16]. For a point-to-point transmission line, double-end traveling wave methods record the arriving time of wave fronts at both terminals and pin-point the fault with both the time differences and the length of the transmission line [17], [18]. In some recent research, the traveling wave-based methods are reported to generate an effective performance in networks with complicate topologies [19].

Since the fault location is calculated with the arriving time of wave fronts and the estimated propagating velocity of traveling surges, accurate calculations of arriving time and propagating velocity of traveling waves are pretty critical. When the traveling wave propagates along long transmission lines, distortion and attenuation occur due to the different velocities of traveling wave components in different frequency bands. However, the velocity used for location is usually taken as a constant and calculated with line parameters measured within a certain frequency band. The calculated velocity used for location analysis might be different from the actual velocity. Also, the recognition of the correct traveling wave is quite crucial for precise location and usually fails when fault location is extremely close to the measuring point because the incident wave will be overlapped by reflected ones. On the other hand, because of attenuations, it is also quite difficult to decide the arrival time of wave fronts from far-away fault points. The location results heavily depend on precise extraction of wave fronts, correct estimation of traveling velocity, and, sometimes, communication quality. As the propagating velocity is close to light speed, a slight error of any factor may result in a large location error.

To reduce the dependence on the precise capturing of the wave front and the correct calculation of propagating velocity, the traveling surges are sometimes characterized by various features which can be recognized by machine learning classifiers. Machine learning is an effective tool in classifying or recognizing labeled or unlabeled data [20]–[23] and has been used in fault location of HVDC system. Some classifiers, including the artificial neural network [21], [24] and extreme learning machine [2], have been employed and have performed well. However, these classifiers require a suitable feature extraction [25]. If the features cannot fully represent the unique differences of traveling waves from different locations, the location results would not be as accurate as expected.

With the emergence of a huge amount of training data and a rapid increase of the computational ability of modern computers, neural networks with unsupervised learning algorithms have been used in tasks such as image processing, natural language processing, etc. in recent years and can provide end-to-end solutions in various cases. It applies various methods such as auto-encoders to learn the features of raw data and avoids the influences from ineffective manual feature extraction, providing an ideal alternative to the traditional machine learning approaches.

Auto-encoder is one of the most popular tools for feature hierarchy. An auto-encoder can learn a representation (encoding) for a set of data with unsupervised learning, and reduce the dimensionality of features. The depth of stacked auto-encoder (SAE) network is relatively shallower than the other deep networks such as conventional neural network. Such a structure is more preferred for analyzing electrical measurements of post-fault procedure of HVDC systems. The use of SAE can avoid complex computations and handle low-dimensional input well.

This paper proposes a stacked auto-encoder (SAE) based end-to-end fault location method for VSC-HVDC transmission lines. First, the generation, propagation, and reflection of traveling waves on HVDC transmission lines are analyzed. Then, the SAE is trained with carefully selected parameters and tested. Finally, the trained SAE is performed with simulated traveling waves, and the location results show that SAE has a high potential to be applied in field applications.

II. TRAVELING WAVES IN HVDC

A. GENERATION AND PROPAGATION OF TWS

The ground fault in power transmission system can be equivalent to a step voltage excitation that is switched on when a fault occurs. Due to the increase of propagation distance or the losses on transmission line resistance, the magnitude of the incident wave front decreases. The impulsive surge will be extended. The longer it propagates, the smoother it is. On the other hand, the amplitude of the traveling wave and the corresponding propagating speed vary with frequency. After a long distance propagation, traveling waves can reach the terminal of transmission line at different instants because of different velocities. The traveling wave fronts measured at the terminals of the transmission line would be distorted during propagation. Fig.1 illustrates the distortion and attenuation of traveling wave fronts after propagating different distances.

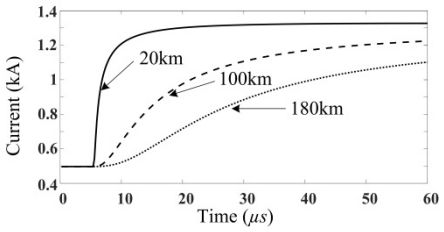

FIGURE 1. Attenuation of traveling surges propagating different distances.

The same ground fault is placed at different distances to illustrate the distortion and attenuation of traveling wave fronts after propagating different distances. As shown in Fig.1, the wave fronts that propagate longer are more extended than those closer to the measuring points.

B. SUCCESSIVE REFLECTIONS OF TW

As with all electromagnetic traveling waves, traveling waves on transmission lines will be reflected and

transmitted at discontinuous junctions. This phenomenon can be described clearly with a lattice diagram, as demonstrated in Appendix A. The successive reflections of traveling waves can be seen from the lattice diagram, at the measuring point, to be a wave train [26]. The interval between two surges in wave train is 2τ, where τ is the duration of the traveling wave propagating from the grounded fault point to the measurement equipment. In power system monitoring, a piece of data segment is often used in analysis. If the data window is shorter than 2τ, only one traveling surge will be captured, otherwise, two or more surges will be recorded. Fig.2 shows traveling waves from four different locations. All of the traveling surges are detected with a certain data window.

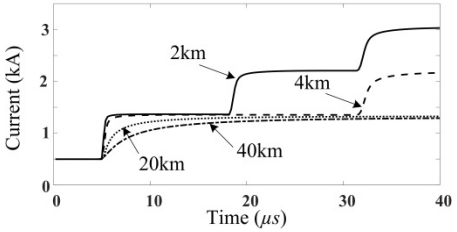

FIGURE 2. Traveling surges from different fault points in a same data window.

For a 40 microsecond data window, as shown in Fig.2, more than one amplitude increase, or traveling surge can be detected if the interval duration τ is smaller than 20μs. Traveling waves are usually regarded to propagate with a speed approaching to 3×10^8m/s, or the speed of light [26]. Thus, the smallest distance for a single traveling surge detection in such a data window is $20\ \mu\text{s} \times 3 \times 10^8\text{m/s} = 6$ km. In Fig.2, the traveling wave trains from faults at 2 and 4 km are clearly demonstrated, while only one traveling wave is captured for faults at 20 and 40 km.

According to the above analysis, the waveform of the traveling wave varies with the distance of the fault. However, due to distortion, attenuation, and reflection, it might be a bit hard to build the relationship between waveform and fault location using linear models. A tool that can deal with complex learning tasks is needed for precise location.

III. FUNDAMENTALS OF THE STACKED AUTO-ENCODER

A stacked auto-encoder (SAE) is actually a kind of neural network with deep learning algorithms [26]–[31]. The aim of an auto-encoder is to learn a representation or encoding for a set of data [27], [32]. SAE uses auto-encoders in the pre-training procedure and uses back-propagation in the fine-tuning stage [31], [33]. Its training procedure is performed layer by layer. Each layer is trained on a set of features extracted by the previous layer. More layers suggest a more complex feature extraction [28]. Fig.3 displays an example structure of SAE. Here, x stands for the inputs, while h stands for features of different layers.

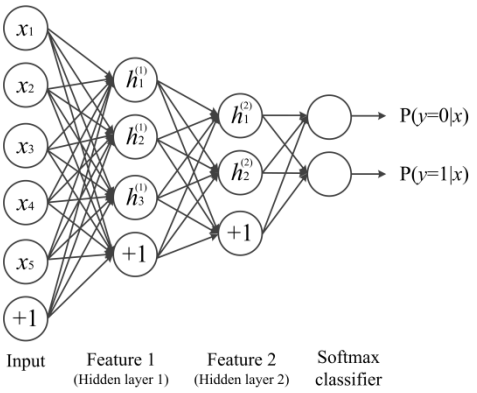

FIGURE 3. An example structure of SAE.

Such feature hierarchy can help SAEs in handling large, high-dimensional data sets and performing automatic feature extraction without human intervention. This is very useful when the number of training samples is limited, i.e., the measured electrical transient signals [34], [35]. It has a high potential to find the relationship between traveling waves and fault locations. In this paper, a SAE net is selected to deal with fault location problems. With suitable selection of network structure and training functions, an SAE can effectively recognize traveling waves from various locations.

IV. SAE-BASED FAULT LOCATION

Since an SAE is capable of handling raw data, the traveling waves on HVDC transmission lines can be used directly as the input of the SAE. Overall, three steps are included in this proposed SAE-based fault location method: raw data processing, SAE training, and fault location calculation.

A. RAW DATA PROCESSING

To capture traveling surges, a higher sampling frequency is needed. Generally, the traveling waves are sampled at a rate higher than 1 Mega samples per second, that is, 1 MHz/s [27]. In order to reveal the high frequency details, the signals analyzed in this paper are sampled at a rate of 5 MHz/s. Different from a traditional current source convertor (CSC) based HVDC, the VSC HVDC system controls voltages instead of currents. Its currents often change quickly and contain more transient information. The current traveling wave is thus considered in this research. A time window is adopted to record traveling surges. The length of the time window is 2τ, where τ is the propagating time of the traveling wave from the fault point to the measuring device.

An SAE cares more about the waveform of traveling waves, rather than their magnitude. The magnitude differences between all raw inputs might cause errors or slow training. Normalization is certainly needed. All signals used as input are normalized to ensure their values distribute between 0 and 1 by dividing them with their maximum value. Similarly, the output which suggests the location of the fault

is normalized by dividing the total length of the transmission line.

B. SAE TRAINING

A back-propagation network with multiple layers of auto-encoder is adopted. Such a network can map any non-linear inputs to their output with minimal computational overheads [28], [29]. To achieve a better performance of SAE, parameters such as architecture and functions are properly selected according to particular application. The performance of the selected SAE is evaluated with errors.

The selected SAE is trained with various samples, which are generated at different locations with different ground resistances.

C. FAULT LOCATION CALCULATION

The trained network is used to locate faults with a small segment of traveling wave waveform. All parameters of raw data—for instance, sampling rates, time window length, and normalization— should be the same as those samples used for training.

V. SELECTION OF FUNCTIONS AND ARCHITECTURE OF SAE

Suitable parameters and functions of SAE are selected for a particular application to reach their best performance. The architecture and functions of the network are selected according to the requirements of the traveling wave-based HVDC fault location.

A. SELECTION OF SAE ARCHITECTURE

1) SIZE OF INPUT AND OUTPUT LAYERS

The input of SAE is the raw data of traveling waves and the output is the location of the fault. As only the wave fronts of traveling surges are employed in analysis, it is much better to choose a short time window to avoid multiple wave fronts in one input. However, too short a data window cannot display the differences between traveling surges from far away faults, where attenuation makes the wave fronts smooth and similar. Here, a data window of 20 microseconds is adopted. So the size of input is 100 when the sampling frequency is 5 MHz/s.

Since only one fault location is related to one input, the size of the output is one.

2) NUMBER OF HIDDEN LAYERS

The depth of a neural network can increase its capability of extracting features when the input size is huge. However, too much layers of hidden nodes can result in slow training or worse recognition results. Training error is a common criterion to evaluate the performance of a trained network. Here, the mean value of maximum error of each training is adopted. Its definition is shown in (1)

$$E_{mme} = \frac{1}{N}\sum_{i=1}^{N} \max(|y_j - d_j|), \quad j = 1, 2, \ldots, M \qquad (1)$$

TABLE 1. Mean maximum errors of trained networks with different numbers of hidden layers.

No. of hidden layers	2	3	4	5
MME	0.002151	0.065535	0.40	0.49

where N is the number of trained networks, i stands for the i^{th} round of training or the i^{th} trained network, y_j is the calculated fault location of j^{th} input, and d_j is the corresponding j^{th} target output. M is the number of training samples. Table 1 lists the mean maximum errors (MMEs) of trained networks with different numbers of hidden layers. For this calculation, the number of training samples M is 72, and the errors are the mean of $N = 10$ trained networks.

As illustrated in Table 1, for an input with 100 values, two hidden layers are enough for application. Thus, the number of hidden layers is chosen to be two.

3) SIZE OF HIDDEN LAYERS

The same method is used to find the suitable size of hidden layers. Since the feature hierarchy extracts unique characteristics from raw data, the size of the hidden layer is supposed to be smaller than its previous one. The size of the first hidden layer, S_1, ranges from 2 (larger than the output layer) to 100 (equal to input layer), and the size of second hidden layer, S_2, ranges from 1 to the size of the corresponding first hidden layer, S_1. Fig.4 illustrates the distributions of MMEs which are calculated with (1). Each error value shown in Fig.4 is generated by 10 trained networks.

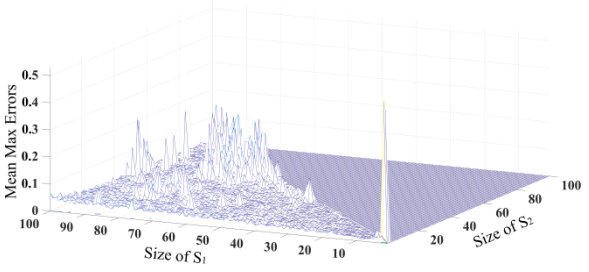

FIGURE 4. MME distribution of networks with different sizes of hidden layers.

As Fig.4 demonstrates, larger sizes of hidden layers are more likely to produce larger errors. According to this error distribution, the network with a 12-node 1st hidden layer and a 12-node 2nd hidden layer is selected, which has the smallest maximum mean error. Therefore, the architecture of the SAE is selected to be 100-12-12-1.

B. SELECTION OF FUNCTIONS

1) ACTIVATION FUNCTION

To effectively extract nonlinear features, activation functions are used to introduce nonlinearity to SAE models. Generally, logistic functions and rectifier functions are often used [30]. Continuous differentiation is a requirement

for gradient-based optimization, like back-propagation [31]. Although rectifier functions are discontinuous, they can still be used in SAE. Logistic activation functions are continuous and are more likely to approach a continuous non-linear model. Here, a sigmoid function is selected to activate hidden layers during unsupervised training and a softmax function, which looks quite similar to the sigmoid function, is used for supervised learning.

2) COST FUNCTION

The goal of using a neural net is to arrive at the point of least error as fast as possible. The most popular cost functions are mean square error (MSE) and cross-entropy function. MSE is the average sum of differences between computed results and targets. It gives too much emphasis on the incorrect outputs when compared with cross entropy, which cares more about closeness of a prediction and is a more granular way to compute error [32].

TABLE 2. MMEs of trained networks with different loss functions

Loss Function	Cross entropy	MSE
MME	0.0138	0.0188

MME, defined by (1), is also used to evaluate the performance of different loss functions. The mean errors of 10 trained networks are listed in Table 2. All parameters of the trained networks, except loss function, are the same. The trained networks with cross entropy can produce smaller errors than those with MSE. Cross entropy is selected in this research.

VI. SIMULATION RESULTS AND COMPARISONS

A. LOCATION RESULTS

In this section, the performance of the proposed SAE-based fault location method is tested with simulated traveling waves. A point-to-point VSC-based transmission system is modeled on the platform of PSCAD/EMTDC. The total length of the DC transmission line is 200 kilometers. The frequency dependent (phase) model is selected to simulate transmission lines. The details of the tower structure model are shown in Appendix B. Two-level AC/DC convertors are adopted. The DC bus voltage is 500 kV and the middle point of the support capacitor is grounded. A single pole to ground fault is simulated and placed at different locations with various ground resistances. Overall, 120 faults are simulated to generate 120 samples. Seventy-two samples are used for training SAE, 18 samples are adopted to test trained network, and the rest (30 samples) are used for fault location. The details of those samples are listed in Table 3.

The size of the SAE is 100-12-12-1. Activation functions are sigmoid and softmax functions for the hidden layers. A cross-entropy function is used as the cost function. The maximum epoch for each training is selected to be 1000. The performance of the trained network is assessed with errors, or the differences between calculated fault locations

TABLE 3. Details of samples

Application	Fault distances (km)	Ground resistance (Ω)	Total numbers
Network Training	2, 4, 20, 40, 80, 100, 120, 160, 180, 196, 198	0, 10, 50, 75, 100	72
Network Testing	2, 4, 20, 40, 80, 100, 120, 160, 180, 196, 198	0, 10, 50, 75, 100	18
Fault Location	5, 65, 95, 105, 135, 195	5, 30, 80, 100	30

(L_{cal}) and actual ones (L_{sim}). The error is defined by (2).

$$E_{err} = |L_{cal} - L_{sim}|/L_{total} \times 100\% \tag{2}$$

Here, L_{total} is the total length of the simulated model, 200 km. To illustrate the range of errors, the mean error and maximum error of a sample group are used. They are defined by following equations

$$E_{err.mean} = \frac{1}{N}\sum_{i=1}^{N} E_{err.i},\ i \in I_N \tag{3}$$

$$E_{err.\max} = \max(E_{err.i}),\ i \in I_N \tag{4}$$

where I_N stands for the sample set, and N is the number of samples.

TABLE 4. Location results of the proposed SAE-based method with similar samples

Fault distance	No. of samples	Mean location error	Maximum location error
$l < 6$ km	2	0.08%	0.10%
6 km $< l \leq 100$ km	8	0.14%	0.31%
$l > 100$km	8	0.16%	0.47%

Table 4 lists the errors of the trained network with similar traveling current waves. Those errors are quite small. All of them are smaller than 0.5%, and the greatest one is only 0.47%. This suggests that the trained network can effectively discriminate the fault locations with raw traveling data and can be used for fault location.

Thirty groups of raw traveling wave data are used for location with trained networks. Those data are totally different from the samples used for training and testing. As fault occurrence in practical applications are random, it is highly possible for a trained network to meet unfamiliar datasets. Table 5 illustrates the location results of the proposed method.

As shown in Table 5, most of the mean location errors are smaller than 1%, and all of the maximum errors are smaller than 2%. For samples that are close to the training samples (5, 95, 105, and 195 km), their location errors are smaller. However, for the samples which are far away from the training samples (65 and 135 km), their errors are larger. Both of their mean errors are greater than 1%. Faults with high

TABLE 5. Location results of the proposed SAE-based method with different samples

Fault distance	No. of samples	Mean location error	Maximum location error
5 km	6	0.31%	0.37%
65 km	6	1.06%	1.13%
95 km	3	0.76%	0.95%
105 km	3	0.75%	0.68%
135 km	6	0.94%	1.23%
195 km	6	0.51%	0.87%

ground resistance are also a challenge in fault location. Larger ground resistance can lead to smaller magnitudes but larger attenuation of current traveling surges. The ground resistance analyzed in Table 5 varies from 5 to 100 Ω. According to the errors listed in Table 5, the proposed SAE-based method can also produce good performance when fault impedances reach up to 100 Ω. For totally unfamiliar raw data, the performance of the SAE is effective enough. By the increasing of the size of training samples, the trained SAE can gain more experience and produce better location results.

B. EFFECT OF NOISES

For practical applications, the detected traveling waves are usually buried in noises. The noises could be interference from nearby electromagnetic devices, impulsive transient interferences, or background Gaussian noises. Most interferences can be removed by de-noising algorithms, for example, lightning disturbances can be eliminated by recognition methods and harmonics can be filtered by hardware. However, Gaussian white noises are usually contained in field tests. The proposed location method is also tested with noised traveling waves. Thirty groups of samples are used in this test. The location results are listed in Table 6.

TABLE 6. Location results of the proposed SAE-based method with different levels of noises

Signal-to-Noise Ratio (SNR)	Mean location error	Max location error
No noises	0.71%	1.23%
60 dB	0.72%	1.36%
50 dB	0.83%	1.78%
40 dB	1.01%	1.97%
30 dB	2.02%	3.84%
20 dB	4.48%	13.63%

According to the location results, the location errors increase with the reduction of SNRs. The maximum location error reaches 13.63% when the SNR is as low as 20 dB. However, the proposed method can perform well when the SNR is up to 40 dB. If de-noising algorithms such as thresholding methods could be used, the location performance can be improved [33].

C. EFFECT OF SYSTEM PARAMETERS

The attenuation of traveling surge fronts mainly depends on the parameters of the DC transmission system, such as transmission line parameters and tower equivalent parameters. Although the training samples can be generated by simulated transmission lines which are modeled precisely, the differences between simulated models and practical systems cannot be avoided. To illustrate the performance of proposed method under slight differences, the system parameters are changed. The details of tested systems are as follows: (1) system A: solid conductor with an outer radius of 0.0203454m, DC resistance $R = 0.03206\Omega$/km; (2) system B: stranded conductor with an outer radius of 0.0203454m, number of strands is 19 and strand radius is 0.003m, DC resistance $R = 0.03206\Omega$/km; and (3) system C: stranded conductor with an outer radius of 0.01438637m, number of strands is 7 and strand radius is 0.0054m, DC resistance $R = 0.06412\Omega$/km. All of the three transmission systems are point-to-point VSC-HVDC transmission lines with a length of 200 kilometers. All of them are simulated with frequency based model (Phase) in PSCAD/EMTDC. For each system, 10 faults are simulated equally on the transmission lines. The location results are listed in Table 7.

TABLE 7. Location results of the proposed SAE-based method with different system parameters

Signal-to-Noise Ratio (SNR)	Mean location error	Max location error
System A	0.71%	1.23%
System B	1.28%	2.12%
System C	2.29%	5.86%

According to the location results, the location errors change with the system parameters. The proposed SAE is trained with samples from system A, and the variation of system parameters can lead to increase of errors. When the system parameters are similar, for example, system A and B, the location results are still effective. But when the system parameters vary a lot, the location errors will increase. The maximum error is 5.86% for system C. For the practical power transmission system with slight differences between simulated models, the performance of SAE based method can be also effective.

D. COMPARISIONS

The goal of this section is to compare the performance of the proposed method with other popular traveling wave-based methods: the single-end arriving time-based method and the traditional artificial neural network (ANN) based method. The traveling wave data used in SAE simulations are also adopted in comparisons.

The single-end traveling wave-based fault location method adopts the arriving time of the incident wave and the reflected wave [34], [35]. According to the lattice diagram of traveling waves in Appendix A, the time difference between incident

wave I_1D and reflected wave $I_1D'BD$ equals to the duration when the traveling wave runs the fault distance twice. With the parameters of the transmission line, it is easy to get the velocity of traveling waves and, thus, the fault distance. However, the precise capturing of traveling wave fronts is very difficult in some cases, for example, when there is noise pollution or large attenuation. In this comparison, wavelet maxima is used to capture the wave fronts of traveling waves. The frequency dependent model of the transmission line is employed and the propagating velocity is calculated to be around 3×10^8m/s.

A traditional ANN-based method often adopts shallow ANN and feature extraction [36]–[38]. Feature selection is quite critical to generate an effective representation of fault signals. Various features are developed, for example, wavelet coefficients, RMS values, a Prony model, and so on. The architecture and functions of ANN are selected carefully with different features and applications. Here, the wavelet confidents of the frequency band 312.5–625 kHz are used as the input of ANN. As the number of wavelet coefficients is 15, a 15-8-1 ANN structure is used. Transfer function ''sigmoid'' and training function ''Levenberg-Marquardt optimization'' are selected.

TABLE 8. Comparison between the proposed method and existing methods

Location Methods	Mean location error	Max location error
Proposed SAE-based method	0.71%	1.23%
Single-end arriving time-based method	2.03%	5.31%
Traditional ANN-based method	1.59%	2.36%

The location results are listed in Table 8. According to these results, both compared methods have larger mean and maximum location errors than the proposed SAE-based one.

VII. CONCLUSIONS

In this paper, an end-to-end fault location method for HVDC transmission lines is presented. With proper selection of parameters and a large amount of raw data as a training sample, SAE is successfully used to solve the fault location problems in an HVDC system with only local current measurements. This method is not affected by the fault position and ground resistance, and shows high reliability and accuracy.

Unlike the traditional traveling wave-based fault location methods in which characteristics need to be carefully selected, the proposed algorithm can process raw data of traveling waves. With more training data available, its performance can even be improved further. The approach presented in this paper is also expected to be a good supplementary to the traveling wave-based fault location methods.

APPENDIX A

The incident waves of a fault move out in opposite directions until they reach the convertor stations, where they reflect as a consequence of the surge impedance of the transmission line boundaries. Reflected waves quickly reach the faulted point where they reflect again as a result of the ground resistance, and some of them transmit into the opposite terminal of the transmission line and then are reflected back. Thus, within a few microseconds the system is alive with a whole series of waves moving in different directions, arriving at different times, of different magnitudes and polarity, and having experienced different attenuations and distortions [26].

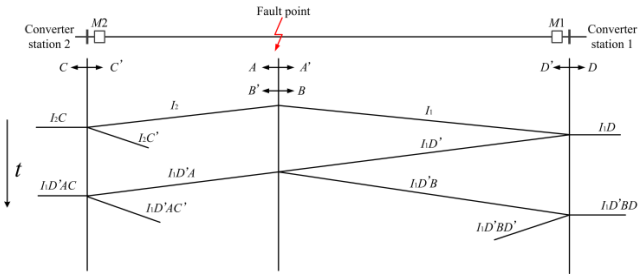

FIGURE 5. The lattice diagram of traveling waves in successive reflections.

In order to keep track of all these components, a lattice diagram has been used, such as that shown in Fig.5. Traveling waves, I_1 and I_2, coming from the fault point, rush towards convertor stations. The characters A, B, C, and D denote the refraction factors, while A', B', C', and D' denote reflection factors. With such a lattice diagram, the progress of each wave component is easily followed as it slides downhill along its zig-zag path. For each measurement device, $M1$ and $M2$, a traveling wave train will be detected, until the currents reach another stable status.

APPENDIX B

Fig. 6 shows the tower structure of the HVDC transmission line model used in this research.

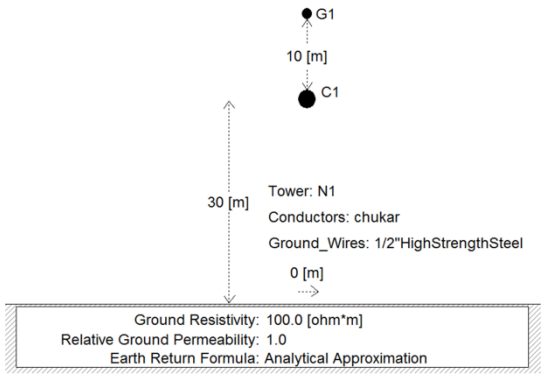

FIGURE 6. Tower structure of the HVDC transmission line.

REFERENCES

[1] N. Flourentzou, V. G. Agelidis, and G. D. Demetriades, ''VSC-based HVDC power transmission systems: An overview,'' *IEEE Trans. Power Electron.*, vol. 24, no. 3, pp. 592–602, Mar. 2009.

[2] Y. Hao, Q. Wang, Y. Li, and W. Song, "An intelligent algorithm for fault location on VSC-HVDC system," *Int. J. Elect. Power Energy Syst.*, vol. 94, pp. 116–123, Jan. 2018.
[3] D. Wang, H. L. Gao, S. B. Luo, and G. B. Zou, "Travelling wave pilot protection for LCC-HVDC transmission lines based on electronic transformers' differential output characteristic," *Int. J. Elect. Power Energy Syst.*, vol. 93, pp. 283–290, Dec. 2017.
[4] M. Li, K. Jia, T. Bi, and Q. Yang, "Sixth harmonic-based fault location for VSC-DC distribution systems," *IET Gener. Transmiss. Distrib.*, vol. 11, no. 14, pp. 3485–3490, Sep. 2017.
[5] J. M. Johnson and A. Yadav, "Complete protection scheme for fault detection, classification and location estimation in HVDC transmission lines using support vector machines," *IET Sci. Meas. Technol.*, vol. 11, no. 3, pp. 279–287, May 2017.
[6] R. Li, L. Xu, and L. Yao, "DC fault detection and location in meshed multiterminal HVDC systems based on DC reactor voltage change rate," *IEEE Trans. Power Del.*, vol. 32, no. 3, pp. 1516–1526, Jun. 2017.
[7] M. Farshad and J. Sadeh, "A novel fault-location method for HVDC transmission lines based on similarity measure of voltage signals," *IEEE Trans. Power Del.*, vol. 28, no. 4, pp. 2483–2490, Oct. 2013.
[8] J. Suonan, S. Gao, G. Song, Z. Jiao, and X. Kang, "A novel fault-location method for HVDC transmission lines," *IEEE Trans. Power Del.*, vol. 25, no. 2, pp. 1203–1209, Apr. 2010.
[9] P. Zhao, Q. Chen, K. Sun, and C. Xi, "A current frequency component-based fault-location method for voltage-source converter-based high-voltage direct current (VSC-HVDC) cables using the S transform," *Energies*, vol. 10, no. 8, p. 1115, Aug. 2017.
[10] M. Daisy, R. Dashti, and H. R. Shaker, "A new fault-location method for HVDC transmission-line based on DC components of voltage and current under line parameter uncertainty," *Elect. Eng.*, vol. 99, no. 2, pp. 573–582, Jun. 2017.
[11] S. Vasanth, Y. M. Yeap, and A. Ukil, "Fault location estimation for VSC-HVDC system using artificial neural network," in *Proc. IEEE Region 10 Conf. (TENCON)* Nov. 2016, pp. 501–504.
[12] R. Perveen, S. R. Mohanty, and N. Kishor, "Fault location in VSC-HVDC section for grid integrated offshore wind farm by EMD," in *Proc. 18th Medit. Electrotechnical Conf. (MELECON)*, E. Kyriakides, E. Kyriacou, G. Ellinas, S. Louca, C. Mavromoustakis, and D. Michael, Eds., Apr. 2016, pp. 1–5.
[13] G. Song, X. Chu, X. Cai, S. Gao, and M. Ran, "A fault-location method for VSC-HVDC transmission lines based on natural frequency of current," *Int. J. Elect. Power Energy Syst.*, vol. 63, pp. 347–352, Dec. 2014.
[14] C. Troitzsch, A.-K. Marten, and D. Westermann, "Non-telecommunication based DC line fault detection methodology for meshed HVDC grids," *IET Gener. Transmiss. Distrib.*, vol. 10, no. 16, pp. 4231–4239, Dec. 2016.
[15] O. M. K. K. Nanayakkara, A. D. Rajapakse, and R. Wachal, "Location of DC line faults in conventional HVDC systems with segments of cables and overhead lines using terminal measurements," *IEEE Trans. Power Del.*, vol. 27, no. 1, pp. 279–288, Jan. 2012.
[16] Z.-Y. He, K. Liao, X.-P. Li, S. Lin, J.-W. Yang, and R.-K. Mai, "Natural frequency-based line fault location in HVDC lines," *IEEE Trans. Power Del.*, vol. 29, no. 2, pp. 851–859, Apr. 2014.
[17] J. Guo, G. Wang, Y. Liang, and D. Zeng, "Global-sensitivity-based theoretical analysis and fast prediction of traveling waves with respect to fault resistance on HVDC transmission lines," *IEEE Trans. Power Del.*, vol. 30, no. 4, pp. 2007–2016, Aug. 2015.
[18] L. Yuansheng, W. Gang, and L. Haifeng, "Time-domain fault-location method on HVDC transmission lines under unsynchronized two-end measurement and uncertain line parameters," *IEEE Trans. Power Del.*, vol. 30, no. 3, pp. 1031–1038, Jun. 2015.
[19] O. M. K. K. Nanayakkara, A. D. Rajapakse, and R. Wachal, "Traveling-wave-based line fault location in star-connected multiterminal HVDC systems," *IEEE Trans. Power Del.*, vol. 27, no. 4, pp. 2286–2294, Oct. 2012.
[20] T. Wu and W. U. Bajwa, "Learning the nonlinear geometry of high-dimensional data: Models and algorithms," *IEEE Trans. Signal Process.*, vol. 63, no. 23, pp. 6229–6244, Dec. 2015.
[21] C. Napoli, G. Pappalardo, G. M. Tina, and E. Tramontana, "Cooperative strategy for optimal management of smart grids by wavelet RNNs and cloud computing," *IEEE Trans. Neural Netw. Learn. Syst.*, vol. 27, no. 8, pp. 1672–1685, Aug. 2016.
[22] T. Wu, P. Gurram, R. M. Rao, and W. U. Bajwa, "Clustering-aware structure-constrained low-rank representation model for learning human action attributes," in *Proc. IEEE 12th Image, Video, Multidimensional Signal Process. Workshop (IVMSP)*, Jul. 2016, pp. 1–5.
[23] S. He and F. Liu, "Resilient fault detection observer design of fuzzy Markovian jumping systems with mode-dependent time-varying delays," *J. Franklin Inst.-Eng. Appl. Math.*, vol. 353, no. 13, pp. 2943–2965, Sep. 2016.
[24] Q. Yang, S. Le Blond, R. Aggarwal, Y. Wang, and J. Li, "New ANN method for multi-terminal HVDC protection relaying," *Electr. Power Syst. Res.*, vol. 148, pp. 192–201, Jul. 2017.
[25] R. J. Hamidi, H. Livani, and R. Rezaiesarlak, "Traveling-wave detection technique using short-time matrix pencil method," *IEEE Trans. Power Del.*, vol. 32, no. 6, pp. 2565–2574, Dec. 2017.
[26] L. V. Bewley, *Traveling Waves on Transmission Systems*. Hoboken, NJ, USA: Wiley, 1951.
[27] G. Luo, Q. Lin, L. Zhou, and J. He, "Recognition of traveling surges in HVDC with wavelet entropy," *Entropy*, vol. 19, no. 5, p. 184, May 2017.
[28] Y. LeCun, Y. Bengio, and G. Hinton, "Deep learning," *Nature*, vol. 521, pp. 436–444, May 2015.
[29] G. Luo, D. Zhang, K. J. Tseng, and J. He, "Impulsive noise reduction for transient Earth voltage-based partial discharge using Wavelet-entropy," *IET Sci. Meas. Technol.*, vol. 10, no. 1, pp. 69–76, Jan. 2016.
[30] J. Patterson and A. Gibson, *Deep Learning: A Practitioner's Approach*. 2017.
[31] J. Snyman, *Practical Mathematical Optimization: An Introduction to Basic Optimization Theory and Classical and New Gradient-Based Algorithms*, 1st ed. New York, NY, USA: Springer, 2005.
[32] J. McCaffrey. (Apr. 22, 2014). *Neural Network Cross Entropy Error, Visual Studio Magazine*. [Online]. Available: https://www.microsoft.com/en-us/research/publication/neural-network-cross-entropy-error/
[33] G. Luo and D. Zhang, "Wavelet denoising," in *Advances in Wavelet Theory and Their Applications in Engineering, Physics and Technology*, D. D. Baleanu, Ed. Rijeka, Croatia: InTech, 2012.
[34] C. Y. Evrenosoglu and A. Abur, "Travelling wave based fault location for teed circuits," *IEEE Trans. Power Del.*, vol. 20, no. 2, pp. 1115–1121, Apr. 2005.
[35] D. Spoor and J. G. Zhu, "Improved single-ended traveling-wave fault-location algorithm based on experience with conventional substation transducers," *IEEE Trans. Power Del.*, vol. 21, no. 3, pp. 1714–1720, Jul. 2006.
[36] R. C. Santos, S. Le Blond, D. V. Coury, and R. K. Aggarwal, "A novel and comprehensive single terminal ANN based decision support for relaying of VSC based HVDC links," *Electr. Power Syst. Res.*, vol. 141, pp. 333–343, Dec. 2016.
[37] J. M. Johnson and A. Yadav, "Fault location estimation in HVDC transmission line using ANN," in *Proc. 1st Int. Conf. Inf. Commun. Technol. Intell. Syst.*, vol. 1, S. C. Satapathy and S. Das, Eds. Cham, Switzerland: Springer, 2016, pp. 205–211.
[38] A. J. Mazon, I. Zamora, J. Gracia, K. J. Sagastabeutia, and J. R. Saenz, "Selecting ANN structures to find transmission faults," *IEEE Comput. Appl. Power*, vol. 14, no. 3, pp. 44–48, Jul. 2001.

GUOMIN LUO received the B.Sc. and M.Sc. degrees from Southwest Jiaotong University, Chengdu, China, in 2005 and 2008, respectively, and the Ph.D. degree from Nanyang Technological University, Singapore, in 2013. She is currently a Lecturer with the School of Electrical Engineering, Beijing Jiaotong University, Beijing, China. Her research areas include the online monitoring of power apparatus, signal processing and time–frequency analysis, and the protection of power systems.

CHANGYUAN YAO is currently a Research Student with the School of Electrical Engineering, Beijing Jiaotong University. His research interests include dc system fault analysis, dc distribution networks, and artificial intelligence.

YINGLIN LIU is currently a Research Student with the School of Electrical Engineering, Beijing Jiaotong University. Her research interests include dc system fault analysis, system modeling, and protection algorithms.

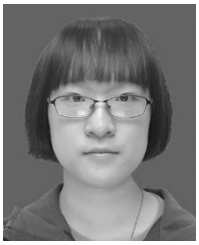

YINGJIE TAN is currently a Research Student with the School of Electrical Engineering, Beijing Jiaotong University. Her research interests include dc system fault location, signal recognition, and artificial intelligence.

JINGHAN HE received the M.S. degree in automation from Tianjing University in 1994 and the Ph.D. degree from Beijing Jiaotong University. She has long been working at the research of online monitoring, protection and control of power systems, power quality, new energy and intelligent power grid, and electrical rail transportation.

KAI WANG received the Ph.D. degree from Nanyang Technological University, Singapore, in 2013. He was with the Huawei Central Research Institute. Since 2016, he has been a Senior Engineer with CloudMinds Technologies Inc. He has published over 10 papers on international journals and conferences. His research interests include deep learning, augmented reality, computer graphics, human–computer interaction, and so on.